*Energies* **2014**, *7*, 5566-5585; doi:10.3390/en7095566

OPEN ACCESS

*energies*

**ISSN 1996-1073**

www.mdpi.com/journal/energies

*Article*

# Differential Protection for an Outgoing Transformer of Large-Scale Doubly Fed Induction Generator-Based Wind Farms

**Bingtuan Gao [1,*], Wei Wei [1], Luoma Zhang [1], Ning Chen [2], Yingjun Wu [3] and Yi Tang [1]**

[1] School of Electrical Engineering, Southeast University, No. 2, Sipailou, Nanjing 210096, Jiangsu, China; E-Mails: weiwei19900212@126.com (W.W.); zhangluoma0614@gmail.com (L.Z.); tangyi@seu.edu.cn (Y.T.)

[2] China Electric Power Research Institute, No. 8, Nanrui Road, Nanjing 210003, Jiangsu, China; E-Mail: chenning8375@163.com

[3] School of Automation, Nanjing University of Posts and Telecommunications, No. 9, Wenyuan Road, Nanjing 210023, Jiangsu, China; E-Mail: ywu_njupt@163.com

* Author to whom correspondence should be addressed; E-Mail: gaobingtuan@seu.edu.cn; Tel.: +86-25-8379-4163; Fax: +86-25-8379-0617.

*Received: 20 June 2014; in revised form: 20 August 2014 / Accepted: 21 August 2014 / Published: 26 August 2014*

---

**Abstract:** With the rapid development of wind energy, relay protection for large-scale wind farms has been attracting some researchers, due to the absence of standards. Based on the large-scale doubly fed induction generator (DFIG)-based wind farms located in Gansu Province, China, this paper studies the differential protection for the outgoing power transformer of large-scale DFIG-based wind farms. According to the equivalent circuit of the power grid integrated with wind farms, the main frequency components of current and voltage during faults are identified mathematically and then verified by simulations. The results show that the frequencies of current and voltage at the terminals of outgoing transmission lines are inconsistent. Following the feature of frequency inconsistency, the adaptability of differential protection is analyzed, and it is found that differential protection for an outgoing transformer in large-scale wind farms may fail once ignoring the frequency inconsistency. Simulation studies demonstrate that inconsistent frequency characteristics will deteriorate the sensitivity and reliability of differential protection. Finally, several suggestions are provided for improving the performance of relay protections for large-scale DFIG-based wind farms.

**Keywords:** wind farm; differential protection; transformer; frequency inconsistency

## 1. Introduction

Wind power has been recognized as one of the most cost-efficient sources of renewable energy [1]. Along with the rapid development of wind turbines, the capacity of a wind farm connected to the power grid is becoming larger and larger. Different technologies regarding utilizing wind energy reliably and efficiently have been studied and developed [1,2]. Additionally, relay protection related to wind turbines and wind farms is a key technology for safe and stable operation of power systems with wind farms. With regard to the setting of relay protection in small-scaled wind farms, the short-circuit current produced by wind turbines during grid faults is always ignored for its insignificant effect on the relay protection; however, it cannot be neglected for a large-scale wind farm, which consists of hundreds of wind turbines. The structure of a typical large-scale DFIG-based wind farm integrated with a power system is shown in Figure 1. When a fault occurs, the frequency of short-circuit current differs from the voltage frequency, which will generate negative effects on traditional transmission relay protection, which gives tacit consent to the uniformity of frequencies of current and voltage [3,4]. Ignoring this short-circuit current will reduce the reliability of its relay protection due to the dynamic behavior of a DFIG-based wind turbine during the period of faults.

**Figure 1.** Structure of a typical large-scale doubly fed induction generator-based wind farm integrated with a power grid.

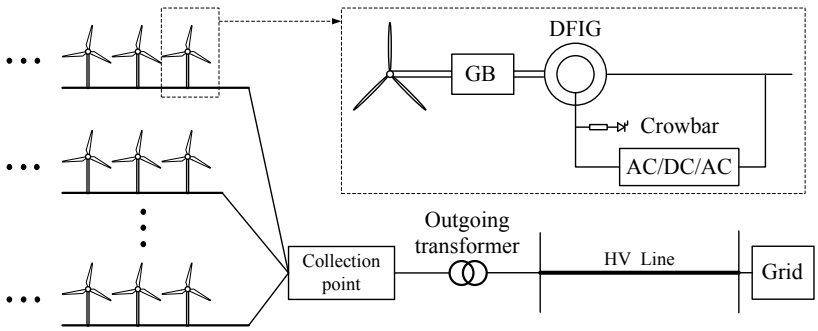


The DFIG-based wind turbine is widely equipped in large wind farms because of its variable rotor speed operation and active and reactive power decoupling control. In order to avoid damage brought by over currents, a rotor-crowbar is required to be quipped for every DFIG to divert current from the rotor-side converter and de-energize the rotor during grid faults [5]. The stator windings of the wound-rotor induction generator are connected to the grid, while the rotor windings are connected to a bidirectional power electronic converter. With a rotor-crowbar, DFIG behaves differently during the period of fault. When voltage sags, the crowbar short-circuits the rotor to protect the converter and the system operating asynchronously. In such a situation, the DFIG is not controlled by the machine-side converter [6]. Short-circuit models for DFIG-based wind turbines have been proposed [7–9], and power system operation with wind farms has also been studied extensively for issues,

such as forecasting [10,11], power control [1,12], grounding [13,14] and fault ride through [15–17]. However, there are still no standardized protection schemes for wind farms, such as those practiced for the protection of conventional generation plants [18].

Some researchers have already studied the relay protection on wind farms. Sarajcev and Goic [19] performed a survey on several important issues, particularly focuses on lightning-initiated surges, for the selection of modern wind farms' over-voltage protection. To prevent maloperation, the setting points of different zones of distance relays change simultaneously with the variation of the wind farm's condition. Sadeghi [20] developed an adaptive unit that adjusts the distance relay's trip characteristic using artificial neural networks with local information. The influences of flexible alternating current transmission system (FACTS) devices on distance relay protection are analyzed in [21], and the Prony method is deployed to improve the constant pickup values based on conventional digital filters [22]. The Prony method is also adopted in [4] to analyze the frequency component of the measured electrical parameters, and the authors utilize a time-domain algorithm based on a differential equation model of a transmission line, which can avoid the frequency issues in distance protection. Since power transformers are extremely important, various protection techniques have been developed [23,24], and differential protection is a commonly used one. Based on the analysis of a transient process using discrete wavelet transformers, an adaptive percentage differential protection is designed for power transformers in [25]. Aiming at the differential protection for a wind farm's outgoing transformer, Zhang *et al.* [26] have uncovered that relay protection on the outgoing transformer with traditional setting values cannot operate correctly, and the failures could be affected by several factors, such as generator type, fault location, fault type and short circuit capacity ratio.

This paper studies the differential protection for the outgoing power transformers in large-scale DFIG-based wind farms connected to the power grid. The network and capacity of the DFIG-based wind farms studied in this paper are based on real wind farms located in Gansu Province in China. We assume that the rotor-crowbar is activated during a short-circuit fault based on the requirement of low-voltage ride through [27,28]. The main contributions of this paper include: (1) the fault behavior of crowbar-protected DFIG-based wind turbines integrated with a power grid is analyzed thoroughly to identify the frequency components of short-circuit current and voltage, which shows the fact that there exists frequency inconsistency for large-scale DFIG-based wind farms integrated with a power grid during faults; (2) following the inconsistent frequency characteristics of the currents, the adaptivity of traditional differential protection on outgoing transformers of large-scale DFIG-based wind farms is investigated and demonstrated with simulations; and (3) several suggestions on improving the reliability of differential protection for large-scale wind farms are proposed.

The rest of the paper is organized as follows. The fault behavior of large-scale DFIG-based wind farms integrated with a power grid is investigated in Section 2, which will show the existence of frequency inconsistency. Following the frequency inconsistency during faults, the adaptivity of differential protection on an outgoing transformer is analyzed in detail in Section 3. Additionally, suggestions on improving the reliability of relay protection in wind farms are provided in Section 4. Finally, conclusions are summarized in Section 5.

## 2. Fault Behavior of Doubly Fed Induction Generator-Based Wind Farms

Since the worst type of short-circuit is a three-phase short-circuit. Here, we take a three-phase symmetric short-circuit as the analyzing case. Other types of short-circuits can be processed similarly.

### *2.1. Crowbar-Protected Doubly Fed Induction Generator-Based Wind Turbines' Response to Fault*

During the period of grid faults, DFIG wind turbines respond in an asynchronous machine operating mode. Morren *et al*. [8] analyzes the behavior of a crowbar-protected DFIG and derives the approximate equations that can be used to determine the short-circuit current contribution of the turbine. The equivalent circuit of the induction machine for transient analysis can be simplified as shown in Figure 2, in which all of the parameters are reduced to the stator side. Additionally, $i_{\mathrm{s}}$ and $i_{\mathrm{r}}$ represent the current of the stator and rotor, respectively; $R_{\mathrm{s}}$ and $R_{\mathrm{r}}$ represent the resistance of the stator and rotor, respectively; $\psi_{\mathrm{s}}$ is the flux of the stator and $\psi_{\mathrm{r}}$ is flux of the rotor; $L_{\mathrm{s}\sigma}$ and $L_{\mathrm{r}\sigma}$ are the leakage inductance of the stator and rotor, respectively; $v_{\mathrm{s}}$ and $v_{\mathrm{r}}$ are the terminal voltage of the stator and rotor, respectively; $L_{\mathrm{m}}$ is the mutual inductance of DFIG; $\omega_{\mathrm{s}}$ and $\omega_{\mathrm{r}}$ represent the rotational speed of stator and rotor, respectively. When the voltage $v_{\mathrm{s}}$ has an angle $\alpha+\frac{\pi}{2}$ with respect to Phase a at the moment the fault occurs, the short-circuit current of Phase a contributed by a DFIG-based wind turbine can be calculated as:

$$i_{\mathrm{sa}} = \frac{\sqrt{2}V_{\mathrm{s}}}{X'_{\mathrm{s}}}\left[e^{-\frac{t}{T'_{\mathrm{s}}}}\cos\alpha - (1-\sigma)\,e^{j\omega_{\mathrm{s}}t}e^{-\frac{t}{T'_{\mathrm{r}}}}\cos\left(\omega_{\mathrm{s}}t+\alpha\right)\right] \tag{1}$$

where parameters $\sigma$, $T'_{\mathrm{s}}$ and $T'_{\mathrm{r}}$ are calculated as:

$$\begin{aligned}
\sigma &= 1-\frac{L_{\mathrm{m}}^2}{L_{\mathrm{s}}L_{\mathrm{r}}}\\
T'_{\mathrm{s}} &= \frac{1}{R_{\mathrm{s}}}\left(L_{\mathrm{s}\sigma}+\frac{L_{\mathrm{r}\sigma}L_{\mathrm{m}}}{L_{\mathrm{r}\sigma}+L_{\mathrm{m}}}\right)\\
T'_{\mathrm{r}} &= \frac{1}{R_{\mathrm{r}}}\left(L_{\mathrm{r}\sigma}+\frac{L_{\mathrm{s}\sigma}L_{\mathrm{m}}}{L_{\mathrm{s}\sigma}+L_{\mathrm{m}}}\right)
\end{aligned}$$

**Figure 2.** Equivalent circuit of an induction machine for transient analysis.

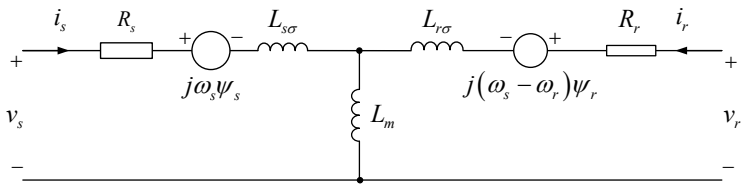


These above equations are achieved with the assumption that the rotor rotates synchronously with the synchronous rotational speed. Actually, the stator short-circuit frequency is determined by the rotor's rotational speed at the moment when the short-circuit occurs.

According to Equation (1), the stator short-circuit current consists of the following two parts:

(1) damping direct current (DC) component $\frac{\sqrt{2}V_{\mathrm{s}}}{X'_{\mathrm{s}}}\left[e^{-\frac{t}{T'_{\mathrm{s}}}}\cos\alpha\right]$ in the stator current.

(2) damping alternating current (AC) component $\frac{\sqrt{2}V_s}{X'_s}\left[-(1-\sigma)\,e^{j\omega_s t}e^{-\frac{t}{T'_r}}\cos(\omega_s t+\alpha)\right]$ in the stator current with a frequency that is determined by the rotor's rotational speed.

### *2.2. Grid Response to Fault*

The short-circuit current contributed by the grid can be presented with the short-circuit current on Phase a:

$$i_{sa} = Ae^{-t/T_s} + B\cos(\omega_0 t + \theta) \tag{2}$$

where $A, B, T_s$ are determined by the network parameters, $\omega_0$ is the frequency of the power grid and $\theta$ is determined by the current phase when the fault occurs. It is straightforward that the short-circuit current provided by the grid can be separated into two parts:

(1) damping DC component $Ae^{-t/T_s}$.

(2) undamped AC component $B\cos(\omega_0 t + \theta)$ with the grid frequency.

### *2.3. Frequency Characteristics of Short-Circuit Current and Voltage*

It has been shown that the frequency of the short circuit current of DIFG during the low-voltage ride-through period deviates from the fundamental frequency according to the operating conditions before the fault [26]. To calculate and analyze the frequency of short-circuit current and voltage, the equivalent circuit network of Figure 1 is given in Figure 3, where $Z_d$ refers to the impedance of the components between DFIG and the outgoing transformer, $Z_g$ refers to the impedance of the components between the grid and the high voltage transmission line and $Z_1$ and $Z_2$ refer to the impedance of the two sizes of transmission line that are separated by the fault. As shown in Figure 3, the overall equivalent circuit network in Figure 3a can be divided into two parts, Figure 3b,c. Additionally, Points A and B are positions to measure the current and voltage values for analysis. We can calculate the current and voltage in these two networks, respectively, and finally add them together to get the result.

**Figure 3.** Equivalent network for short-circuit analysis. (**a**) Wind farm and grid; (**b**) wind farm; (**c**) grid.

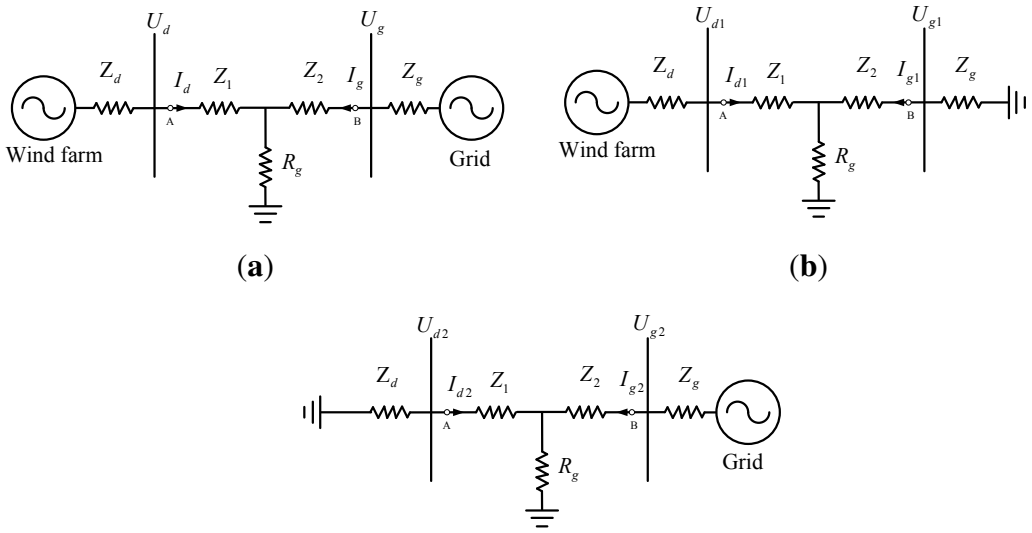

In the network, we assume that $Z_{\mathrm{d}}$ is much larger than others and $Z_{\mathrm{g}}$ is much smaller than others, based on the fact that $Z_{\mathrm{d}}$ represents the components on the lowest voltage level and $Z_{\mathrm{g}}$ represents the components on the highest voltage level. Thus, $|I_{\mathrm{g2}}| \gg |I_{\mathrm{d1}}|$.

According to Section 2.1 and 2.2, $I_{\mathrm{d1}}$ consists of a damping DC component and a damping AC component in the frequency $f_{\mathrm{r}}$ (rotor frequency), while $I_{\mathrm{g2}}$ consists of a damping DC component and a constant AC component in the frequency $f_0$ (grid frequency). According to Figure 3, the following voltage and current equations can be deduced based on Kirchhoff's Law.

$$
\begin{aligned}
I_{\mathrm{g}} &= I_{\mathrm{g1}} + I_{\mathrm{g2}} && (3)\\
I_{\mathrm{d}} &= I_{\mathrm{d1}} + I_{\mathrm{d2}} && (4)\\
U_{\mathrm{d}} &= U_{\mathrm{d1}} + U_{\mathrm{d2}} && (5)\\
U_{\mathrm{g}} &= U_{\mathrm{g1}} + U_{\mathrm{g2}} && (6)\\
I_{\mathrm{g1}} &= \frac{-I_{\mathrm{d1}} R_{\mathrm{g}}}{R_{\mathrm{g}} + Z_2 + Z_{\mathrm{g}}} && (7)\\
I_{\mathrm{d2}} &= \frac{-I_{\mathrm{g2}} R_{\mathrm{g}}}{R_{\mathrm{g}} + I_1 + Z_{\mathrm{d}}} && (8)\\
U_{\mathrm{d1}} &= I_{\mathrm{d1}} \left( Z_1 + \frac{R_{\mathrm{g}} (Z_2 + Z_{\mathrm{g}})}{R_{\mathrm{g}} + Z_2 + Z_{\mathrm{g}}} \right) && (9)\\
U_{\mathrm{g2}} &= I_{\mathrm{g2}} \left( Z_2 + \frac{R_{\mathrm{g}} (Z_1 + Z_{\mathrm{d}})}{R_{\mathrm{g}} + Z_1 + Z_{\mathrm{d}}} \right) && (10)\\
U_{\mathrm{g1}} &= -I_{\mathrm{g1}} Z_{\mathrm{g}} && (11)\\
U_{\mathrm{d2}} &= -I_{\mathrm{d2}} Z_{\mathrm{d}} && (12)
\end{aligned}
$$

Substituting Equation (7) into Equation (3), we have:

$$
I_{\mathrm{g}} = \left( \frac{-I_{\mathrm{d1}}}{I_{\mathrm{g2}}} \frac{R_{\mathrm{g}}}{R_{\mathrm{g}} + Z_2 + Z_{\mathrm{g}}} + 1 \right) I_{\mathrm{g2}} \approx I_{\mathrm{g2}} \tag{13}
$$

Assume $R_{\mathrm{g}}$ is large enough. Substituting Equation (8), Equation (9) and Equation (12) into Equation (5), we have:

$$
\begin{aligned}
U_{\mathrm{d}} &= \left\{ \frac{R_{\mathrm{g}}}{\frac{R_{\mathrm{g}}}{Z_{\mathrm{d}}} + \frac{I_1}{Z_{\mathrm{d}}} + 1} + \frac{I_{d1}}{I_{\mathrm{g2}}} \left[ Z_1 + \frac{R_{\mathrm{g}} (Z_2 + Z_{\mathrm{g}})}{R_{\mathrm{g}} + Z_2 + Z_{\mathrm{g}}} \right] \right\} I_{\mathrm{g2}} \\
&\approx R_{\mathrm{g}} I_{\mathrm{g2}} && (14)
\end{aligned}
$$

Assume $R_{\mathrm{g}}$ is close to zero; we have:

$$
U_d = I_{d1} Z_1 \tag{15}
$$

Substituting Equation (7), Equation (10) and Equation (11) into Equation (6), we have:

$$
\begin{aligned}
U_{\mathrm{g}} &= \left[ \frac{I_{\mathrm{d1}}}{I_{\mathrm{g2}}} \frac{R_{\mathrm{g}} Z_{\mathrm{g}}}{R_{\mathrm{g}} + Z_2 + Z_{\mathrm{g}}} + Z_2 + \frac{R_{\mathrm{g}} \left( \frac{Z_1}{Z_{\mathrm{d}}} + 1 \right)}{\frac{R_{\mathrm{g}}}{Z_{\mathrm{d}}} + \frac{Z_1}{Z_{\mathrm{d}}} + 1} \right] I_{\mathrm{g2}} \\
&\approx (Z_2 + R_{\mathrm{g}}) I_{\mathrm{g2}} && (16)
\end{aligned}
$$

Substituting Equation (8) into Equation (4), we have:

$$I_{\mathrm{d}} = I_{\mathrm{d1}} - \left( \frac{\frac{R_{\mathrm{g}}}{Z_{\mathrm{d}}}}{\frac{R_{\mathrm{g}}}{Z_{\mathrm{d}}} + \frac{Z_{\mathrm{l}}}{Z_{\mathrm{d}}} + 1} \right) I_{\mathrm{g2}} \approx I_{\mathrm{d1}} - \frac{R_{\mathrm{g}}}{Z_{\mathrm{d}}} I_{\mathrm{g2}} \tag{17}$$

Therefore, it can be concluded that the main frequency component of $I_{\mathrm{d}}$ is determined by $R_{\mathrm{g}}$.

Since relay protection cares about the AC components of fault current, we neglect the DC components in the following sections.

To summarize, the frequency characteristic of short-circuit current and voltage on the transmission line is concluded in Table 1.

**Table 1.** The analyzed main frequency of the short-circuit current and voltage.

| **Parameters** | $R_{\mathrm{g}}$ **close to 0** | $R_{\mathrm{g}}$ **not close to 0** |
|---|---|---|
| $I_{\mathrm{g}}$ | $f_0$ | $f_0$ |
| $I_{\mathrm{d}}$ | $f_{\mathrm{r}}$ | undetermined |
| $U_{\mathrm{g}}$ | $f_0$ | $f_0$ |
| $U_{\mathrm{d}}$ | $f_{\mathrm{r}}$ | $f_0$ |

In the following subsection, this result will be verified by simulations and a more explicit relationship between $R_g$, and the fault current's frequency characteristics will also be demonstrated.

### *2.4. Simulation Analysis on Frequency Inconsistency*

In MATLAB/Simulink, we build the simulation mode of a wind farm integrated with the power grid located in Gansu Province in China, as shown in Figure 4. DIFG-based wind turbines are connected to a 35-kV bus with box transformers, whose rated power is 1.5 MW. The percentage of short-circuit voltage is selected as 6%. The collection bus is 10 km long with a positive sequence impedance 0.1 + *j*0.3 Ω/km and a zero sequence impedance 0.3 + *j*0.9 Ω/km. The outgoing transformer 35/330 kV transmits power from the wind farm through 330 kV transmission line to the 330/500 kV transformer connected to the power grid. The rated power for the outgoing transformer 35/330 kV is 220 MW. The percentage of impedance voltage is 20%. The transmission line is 20 km long with a positive sequence impedance 0.1 + *j*0.4 Ω/km and a zero sequence impedance 0.3 + *j*1.2 Ω/km. The rated power of the transformer 330/500 kV is 240 MW, and its percentage of impedance voltage is 24%.

**Figure 4.** The simulation case based on real wind farms located in Gansu province in China.

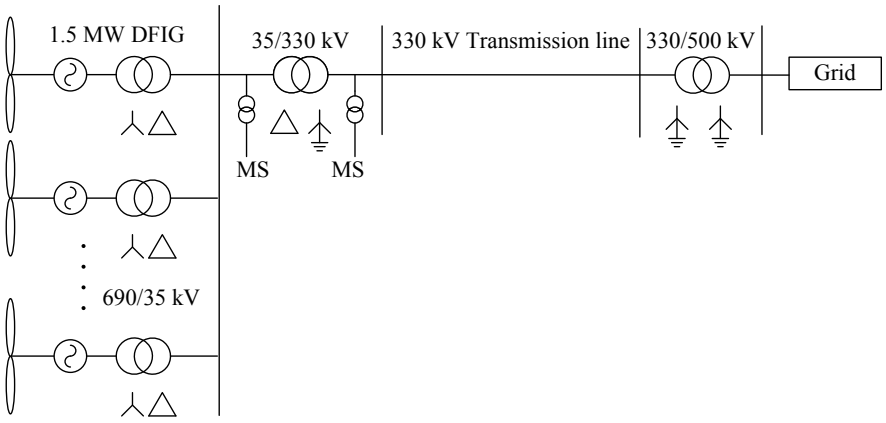

To study the frequency inconsistency discussed in the last subsections, the size of the wind farm is selected as 138 × 1.5-MW DIFG-based wind turbines. A three-phase fault occurs on the transmission line at the terminal of the outgoing transformer, and the DFIG rotor's rotational frequency is 35 Hz, with the grid frequency maintains at 50 Hz. Different values of $R_g$ have been adopted in the simulation to observe the characteristics of short-circuit current and voltage. To study the magnitude of current and voltage with different frequencies clearly, fast Fourier transformation (FFT) is deployed to analyze $I_{\mathrm{d}}, I_{\mathrm{g}}, U_{\mathrm{d}}$ and $U_{\mathrm{g}}$ for the cases of $R_{\mathrm{g}}$ = 0 Ω, $R_{\mathrm{g}}$ = 10 Ω and $R_{\mathrm{g}}$ = 100 Ω in the interval of 0.2 s after the fault occurred. The results are shown in Table 2.

**Table 2.** Fast Fourier transformation analysis of currents and voltages with 138 wind turbines.

| $R_{\mathrm{g}}$ | Variables | Mag of 35 Hz wave | Mag of 50 Hz wave | Percentage of 35 Hz |
|---|---|---|---|---|
| 0 Ω | $I_{\mathrm{d}}$ | 131.1 | 39.46 | 77.13% |
| | $I_{\mathrm{g}}$ | 7.74 | 1,804 | 0.43% |
| | $U_{\mathrm{d}}$ | 759.5 | 309.2 | 71.07% |
| | $U_{\mathrm{g}}$ | 26.81 | 26.81 | 50.00% |
| 10 Ω | $I_{\mathrm{d}}$ | 137 | 19.16 | 87.73% |
| | $I_{\mathrm{g}}$ | 25.35 | 1,790 | 1.39% |
| | $U_{\mathrm{d}}$ | 1,737 | $17.7 \times 10^3$ | 8.94% |
| | $U_{\mathrm{g}}$ | 1,226 | $17.9 \times 10^3$ | 6.41% |
| 100 Ω | $I_{\mathrm{d}}$ | 152.3 | 330.1 | 31.57% |
| | $I_{\mathrm{g}}$ | 124.7 | 1,407 | 8.14% |
| | $U_{\mathrm{d}}$ | 9,777 | $119.6 \times 10^3$ | 7.56% |
| | $U_{\mathrm{g}}$ | 8,920 | $122.3 \times 10^3$ | 6.80% |

The results in Table 2 demonstrate that the main frequency component of the current $I_{\mathrm{g}}$ and voltage $U_{\mathrm{g}}$ at the transmission line terminal near the grid side is always 50 Hz whatever the size of transition resistance $R_{\mathrm{g}}$ is. However, for the the current $I_{\mathrm{d}}$ and voltage $U_{\mathrm{d}}$ at the transmission line terminal near the DIFG-based wind farm side, when transition resistance $R_{\mathrm{g}}$ = 0 Ω, the main frequency component is 35 Hz. As the size of the transition resistance $R_{\mathrm{g}}$ increases, the amount of the 50-Hz frequency component of $U_{\mathrm{d}}$ increases more than that of $I_{\mathrm{d}}$. In the case of $R_g$ = 100 Ω, the main frequency component of all $I_{\mathrm{d}}, I_{\mathrm{g}}, U_{\mathrm{d}}$ and $U_{\mathrm{g}}$ is 50 Hz. By comparing the FFT analysis result in Table 2 with the analyzing result in Table 1 in the last subsection, one can find that the simulation results are consistent with the mathematical analysis results. This proves that there exists frequency inconsistency during the period of outgoing transmission line fault occurring in the power grid integrated with the DFIG-based wind farm.

To study how the capacity of a wind farm affects the frequency inconsistency, a simulation is implemented with the same wind farm-integrated power grid with different numbers of wind turbines. In this simulation, the number of wind turbines is reduced to 69 from 138. The results are given in Table 3. One can see that when the capacity of the wind farm decreases, the main frequency component of $I_{\mathrm{d}}$ changes very little, while $I_{\mathrm{g}}, U_{\mathrm{d}}$ and $U_{\mathrm{g}}$ have a lesser amount of the 35-Hz component.

**Table 3.** Fast Fourier transformation analysis of currents and voltages with 69 wind turbines.

| $R_g$ | Variables | Mag of 35 Hz wave | Mag of 50 Hz wave | Percentage of 35 Hz |
|---|---|---|---|---|
| 0 Ω | $I_d$ | 66.59 | 19.9 | 77.00% |
| | $I_g$ | 4.32 | 1,806 | 0.24% |
| | $U_d$ | 394 | 163.1 | 71.72% |
| | $U_g$ | 26.84 | 26.84 | 50.00% |
| 10 Ω | $I_d$ | 68.23 | 9.185 | 88.14% |
| | $I_g$ | 15.35 | 1,794 | 0.84% |
| | $U_d$ | 847.6 | $17.87 \times 10^3$ | 4.53% |
| | $U_g$ | 581.6 | $17.95 \times 10^3$ | 3.14% |
| 100 Ω | $I_d$ | 76.01 | 184.1 | 29.22% |
| | $I_g$ | 71.26 | 1,428 | 4.75% |
| | $U_d$ | 3,946 | $131.8 \times 10^3$ | 2.90% |
| | $U_g$ | 3,944 | $133.3 \times 10^3$ | 2.56% |

## 3. Adaptability of the Differential Protection

### *3.1. Differential Protection*

Typical differential protection for outgoing transformers consists of three parts, including percentage differential protection, second harmonic restraint protection and over-current differential protection. The logical relationship of the protections is depicted in Figure 5.

**Figure 5.** Protection logic of the outgoing transformer.

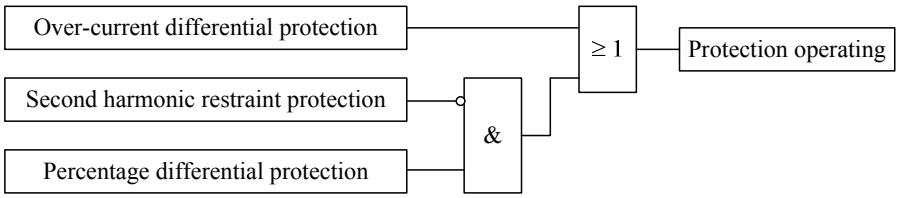


#### 3.1.1. Percentage Differential Protection

The classic operating criteria for percentage differential protection [23,26] can be expressed as the following equations and inequalities.

$$\begin{cases} I_{op} > I_{op.0} & I_{res} \le I_{res.0} \\ I_{op} \ge I_{op.0} + k\left(I_{res} - I_{res.0}\right) & I_{res} \ge I_{res.0} \\ I_{op} = \left|\vec{I}_1 + \vec{I}_2\right| \\ I_{res} = \left|\vec{I}_1 - \vec{I}_2\right| / 2 \end{cases} \tag{18}$$

where different current (also called operating current), $I_{op}$, is obtained as the phase sum of currents entering the protection element $\vec{I}_1$ and $\vec{I}_2$, $I_{op.0}$ is the threshold for avoiding maloperation when the

restraint current $I_{\text{res}}$ is close to zero, $I_{\text{res.0}}$ is the minimal restraint current and $k$ is called the constraint coefficient, which could be set to a value between zero or one. The criteria given in Equation (18) can be depicted as in Figure 6. The protection operating region is the shadow area where the inequalities of criteria Equation (18) are satisfied.

**Figure 6.** Operation zone of percentage differential protection.

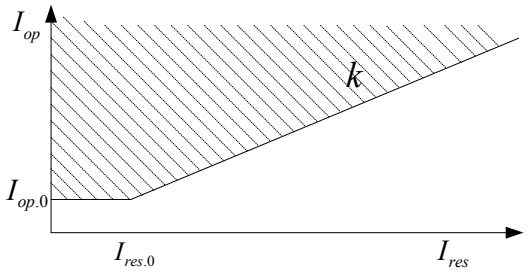


3.1.2. Second Harmonic Restraint Protection

Any transient in the transformer circuit can generate inrush current. For example, when a transformer is energized, a large inrush current accompanied by a non-ignorable second harmonic wave would be drawn by the transformer. In order to prevent the protection from maloperation, the second harmonic wave restraint protection is employed in differential protection for the outgoing transformer.

The criteria of the second harmonic wave restraint protection is defined as:

$$K=\frac{I_2}{I_1} \tag{19}$$

where $I_2$ refers to the amplitude of the second harmonic component (100 Hz) in the differential current, while $I_1$ refers to the amplitude of the fundamental frequency component (50 Hz). By comparing the real-time value of $K$ with a setting value, it can be detected if a real fault occurs or not.

3.1.3. Over-Current Differential Protection

Over-current differential protection is applied to clear faults. Its setting value should be larger than both the inrush current of the transformer and the transient unbalanced current resulting from external faults.

*3.2. Adaptability Analysis*

For differential protection, the magnitudes of current and voltage vectors are usually processed by Fourier transformation. Fourier transformation analysis on power systems usually takes the grid frequency as its fundamental frequency. Therefore, the magnitudes of any inharmonic waves fluctuate with time. If $I_{\text{d}}$ and $I_{\text{g}}$ steadily stay with grid frequency, the values of $I_{\text{op}}$ and $I_{\text{res}}$ remain constant, and thus, the protection performs well. However, when transmission line faults, that is, the typical ground faults discussed here, occur in a large wind farm, especially for those grounded with low resistance, the short-circuit current contributed by DFIG wind turbines deviates from grid frequency, which may result in failures of the differential protection.

These negative influences on the mentioned three parts of differential protection will be analyzed respectively.

3.2.1. Influences on Percentage Differential Protection

Zhang *et al.* [4] has pointed out that the amplitude of the current with frequency differing from the fundamental frequency fluctuates with time when it is processed by the Fourier transformation. Therefore, when the fault current's frequency deviates, the differential current and the breaking current go across each other, which results in the delay of protection. To observe this effect straightforwardly, a simplified model with two signals, $i_1 = 5\sin 70\pi t$ and $i_2 = 10\sin 100\pi t$, is used for simulation here. The simulation result in Figure 7 shows that both $I_{op}$ and $I_{res}$ fluctuate with time and intersect with each other periodically, which significantly deteriorates the reliability of protection.

**Figure 7.** $I_{res}$ and $I_{op}$.

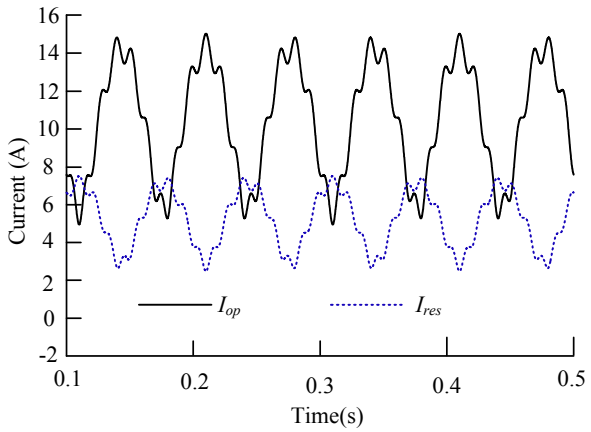


To further study the adaptivity of the percentage differential protection in DIFG-based wind farms integrated to power grid, a large-scale wind farm containing 200 ×1.5-MW DFIG-based wind turbines integrated with a power grid was built and simulated in MATLAB/Simulink. The simulation result is shown in Figure 8. The arrows in Figure 8 indicate the varying trajectory of differential current. It shows that the inconsistent frequency feature of $I_g$ and $I_d$ during faults has a negative impact on the percentage differential protection. The trajectory crosses the operation action line back and forth several times, which reflects the unreliability and low sensitivity of the protection.

**Figure 8.** Differential current and restraint current.

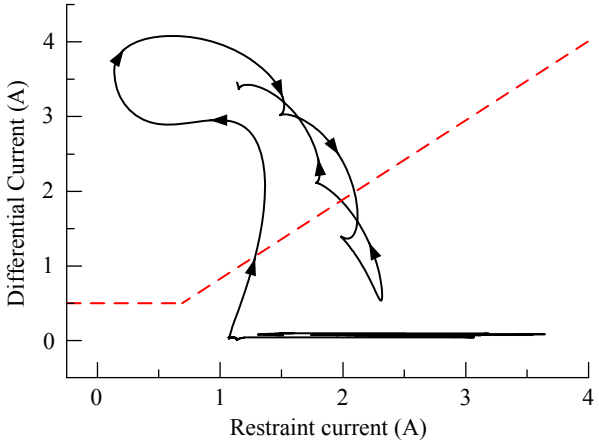

It should be noted that most of the parameters in the simulation are set to meet the worst situation to observe the negative effect. For example, zero resistance fault occurs at the terminal of the transmission line near the wind turbines, which means that the frequency inconsistency reaches its maximum. However, although the studied scenario is some extreme case with worse parameters, it should be considered for protection design in practical DFIG-based wind farms.

3.2.2. Influences on Second Harmonic Restraint

To simplify the problem, we ignore the DC component in the current and assume that its amplitude does not decrease with time. The wind farm side current is described as a sine wave signal with amplitude one and frequency $\omega_r$:

$$i_d(t) = \sin(\omega_r t + \varphi) \tag{20}$$

The grid side current with amplitude $A$ and frequency $\omega_r$ is described in the following expression.

$$i_g(t) = A\sin(\omega_s t + \varphi) \tag{21}$$

Additionally, the the differential current is:

$$i_{op}(t) = i_d(t) + i_g(t) \tag{22}$$

By taking $\omega_s$ as the fundamental frequency and doing a Fourier transformation to $i_{op}$, we can get the following two second harmonic components of the differential current:

$$\begin{aligned} I_{2\cos} &= \frac{\omega_s}{\pi}\int_{-\pi/\omega_s}^{\pi/\omega_s} i_{op}(t)\cos(2\omega_s t)dt = \frac{2\frac{\omega_r}{\omega_s}\sin\varphi\sin(\frac{\omega_r}{\omega_s}\pi)}{\pi\left[\left(\frac{\omega_r}{\omega_s}\right)^2-4\right]} \\ I_{2\sin} &= \frac{\omega_s}{\pi}\int_{-\pi/\omega_s}^{\pi/\omega_s} i_{op}(t)\sin(2\omega_s t)dt = \frac{4\cos\varphi\sin(\frac{\omega_r}{\omega_s}\pi)}{\pi\left[\left(\frac{\omega_r}{\omega_s}\right)^2-4\right]} \end{aligned}$$

Finally, the second harmonic component can be obtained by adding the two parts together:

$$I_2 = \frac{\sin(\lambda\pi)}{\pi(\lambda^2-4)}\sqrt{(2\lambda)^2+[16-(2\lambda)^2]\cos^2(\varphi)} \tag{23}$$

where $\lambda = \frac{\omega_r}{\omega_s}$.

Similarly, the amplitude of fundamental wave can be calculated in the same way. Therefore, we can get $K$ according to Equation (19).

$$K = \frac{\frac{(1-\lambda^2)\sin(\lambda\pi)}{(\lambda^2-4)}\sqrt{(2\lambda)^2+[16-(2\lambda)^2]\cos^2\omega_r t}}{\sqrt{[2\lambda\sin(\omega_r t)\sin(\lambda\pi)+A\pi(1-\lambda^2)\sin(\omega_s t)]^2+[2\cos(\omega_r t)\sin(\lambda\pi)+A\pi(1-\lambda^2)\cos(\omega_s t)]^2}} \tag{24}$$

A similar simulation system as described in Section 2.4 was built in MATLAB/Simulink. The number of wind turbines is selected as 150; the slip ratio is set to 0.3; the setting value of second harmonic

restraint is 0.12; and a three-phase grounding fault occurs at 0.505 s. The simulation result is shown in Figure 9. At the instant the fault occurs, the values of $K$ for all three phases are larger than the setting value, and then, the protection is blocked. Until the instant of 0.522 s, all of the values of $K$ decrease and are smaller than the setting value. This means that the percentage differential protection remains blocked from 0.505 s to 0.522 s, and it will not respond to faults, whether the action condition is met or not. That is to say, the operating action is delayed about 17 ms.

**Figure 9.** Simulation result on second harmonic restraint protection.

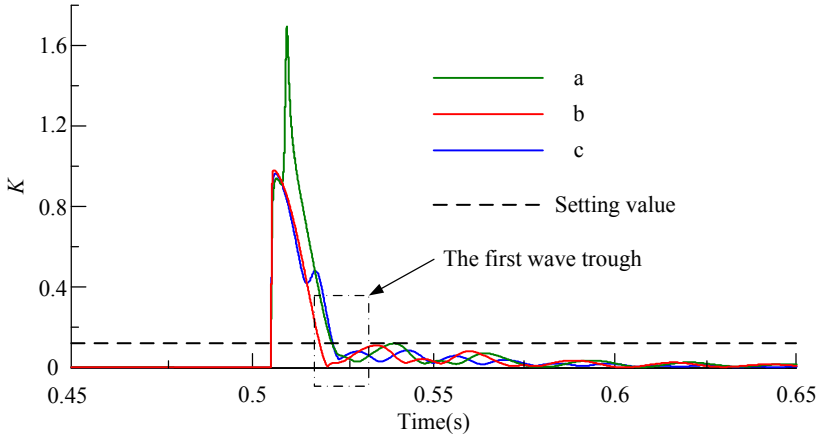


Another observation based on the simulation result given in Figure 9 is that whether the protection would be unblocked successfully depends on the minimum $K$ at the first wave trough. If the values of $K$ at the first wave trough are still larger than the setting value, the protection will remain blocked, and the action instant of protection will be delayed more. Therefore, there is a need to study the impacts of the minimal value of $K$, *i.e.* $K_{\min}$, on the protection. For $A \in [1.2, 3]$ and $\lambda \in [0.5, 3.5]$, according to Equation (24), Figure 10 can be obtained.

**Figure 10.** Minimal value of $K$.

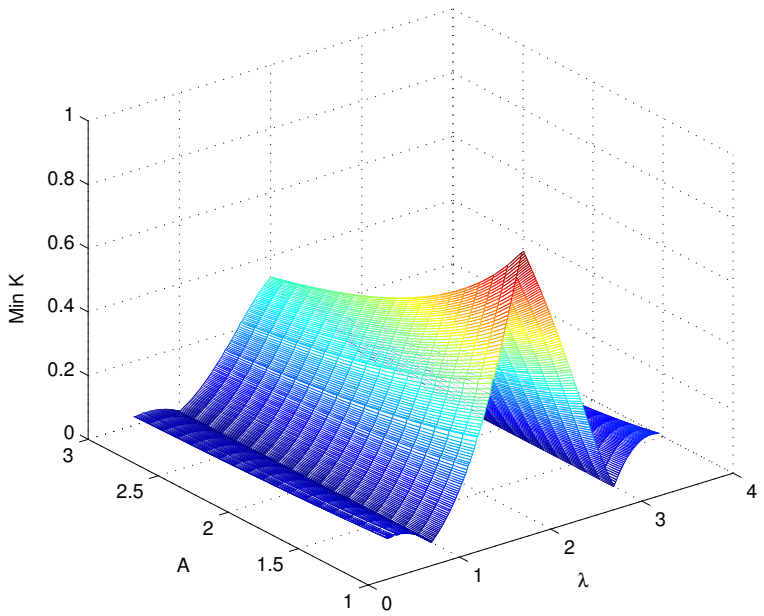

According to Figure 10, for a constant λ, $K_{\min}$ increases, while $A$ decreases; for a constant $A$, $K_{\min}$ becomes smaller when λ gets closing to one or three. Normally, the value of λ is in the range $[0.7, 1.3]$ for a practical DFIG-based wind farm. This means that the larger capacity the wind farm owns and the more current frequency deviates from the power frequency, the larger $K_{\min}$ is, which indicates the larger possibility for the protection to be delayed. Moreover, it can be concluded that when DFIG operates at a super-synchronization speed, *i.e.*, $\lambda > 1$, a more significant negative effect on relay protection could be brought.

#### 3.2.3. Influences on Over-Current Differential Protection

When $\omega_r = \omega_s$, the maximum value of differential current equals $1 + A$. When $\omega_r \neq \omega_s$, the differential current fluctuates. For over-current differential protection, we are concerned with the maximum amplitude of the current only. Given that $A = 1.5$, the maximum amplitude of the differential current with respect to λ is illustrated in Figure 11.

**Figure 11.** Maximum amplitude characteristics of a differential current.

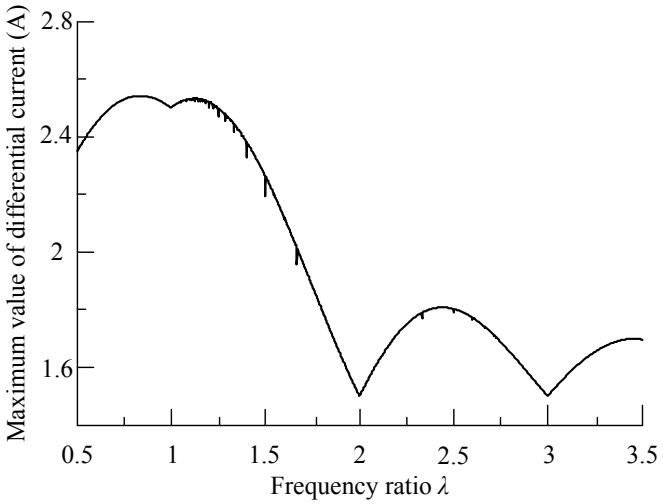


It is clear according to Figure 11 that, for a fixed constant $A$, when λ fluctuates in a small range around one, the amplitude of the differential current increases and exceeds 2.5, which means that the over-current differential protection is even more sensible. When the derivation of the current frequency keeps growing, *i.e.*, the frequency ratio λ keeps deviating by one, the sensibility of the over-current differential protection falls.

## 4. Improving the Reliability of Relay Protection in Wind Farms

According to the analysis and discussion in the last two sections, there are four main factors that affect the reliability and sensibility of protections in large-scale wind farms: (1) the capacity of the wind farm; (2) the frequency deviation; (3) the transition impedance; and (4) the types of short-circuits. In this section, a conclusion about how these factors affect the relay protection and the ways corresponding to improving the reliability of the protection will be provided.

### *4.1. Factors Affecting the Reliability of Relay Protection*

#### 4.1.1. Types of Short-Circuits

Relevant values of differential current and restraint current are employed to make comparisons for percentage differential protection. For different types of short-circuits, the differential current and restraint current increase or decrease simultaneously. This leads to less impact on the percentage of differential protection. A similar conclusion can be drawn to the second harmonic restraint protection. However, since the over-current differential protection is to compare the absolute maximum amplitude of the differential current with a setting value, the three-phase short-circuit can generate the largest amplitude of short-circuit current, which can activate the relay operation much more easily.

#### 4.1.2. Transition Impedance

According to the analysis in Section 2.3 and the demonstration in Section 2.4, a smaller transition impedance leads to a larger percentage of the frequency deviation component of the short-circuit current. Therefore, when a fault occurs with a transition impedance that cannot be ignored, such as non-metal-grounding, the main frequency component of the short-circuit current is fundamental frequency. In such a case, the Fourier transformation can extract the components more precisely because of the lesser second harmonic component, and more reliable protection can be achieved.

#### 4.1.3. Wind Farm Capacity and Frequency Deviation

The wind farm's capacity depends on the number of DFIG-based wind turbines connected to the gird, and the frequency deviation depends on the DFIG's operating condition at the instant a fault occurs. We have demonstrated in Section 2.4 that the smaller capacity of wind farms does not change the frequency deviation of short-circuit current near the terminal of the wind farm side. To observe how the wind farm capacity and frequency derivation affect the second harmonic restraint protection, the relationship between the time delay of protection with the short-circuit capacity ratio of the wind farm, which is defined as the wind farm's short-circuit capacity divided by the grid's capacity, and the slip ratio of DFIG is plotted in Figure 12, where the setting value of the second harmonic restraint protection is selected as $K = 0.12$.

From Figure 12, we can see that for a constant slip ratio of the DFIG, a larger wind farm capacity results in a longer protection time delay. A DFIG operated at a super-synchronous speed can cause a longer protection time delay than a sub-synchronous speed. The reason lying behind, for the same absolute slip ratio, is that the minimal second harmonic ratio $K$ of super-synchronous operation is much larger than the one for sub-synchronous operation. Another observation is that mutation time delays happens. This is because the second harmonic restraint value $K$ is larger than the setting value 0.12 at the first wave trough. Additionally, the protections will be blocked until the value of $K$ is smaller than the setting value 0.12 at the second wave trough.

**Figure 12.** Time delay of protection with the setting value of $K$ selected as 0.12.

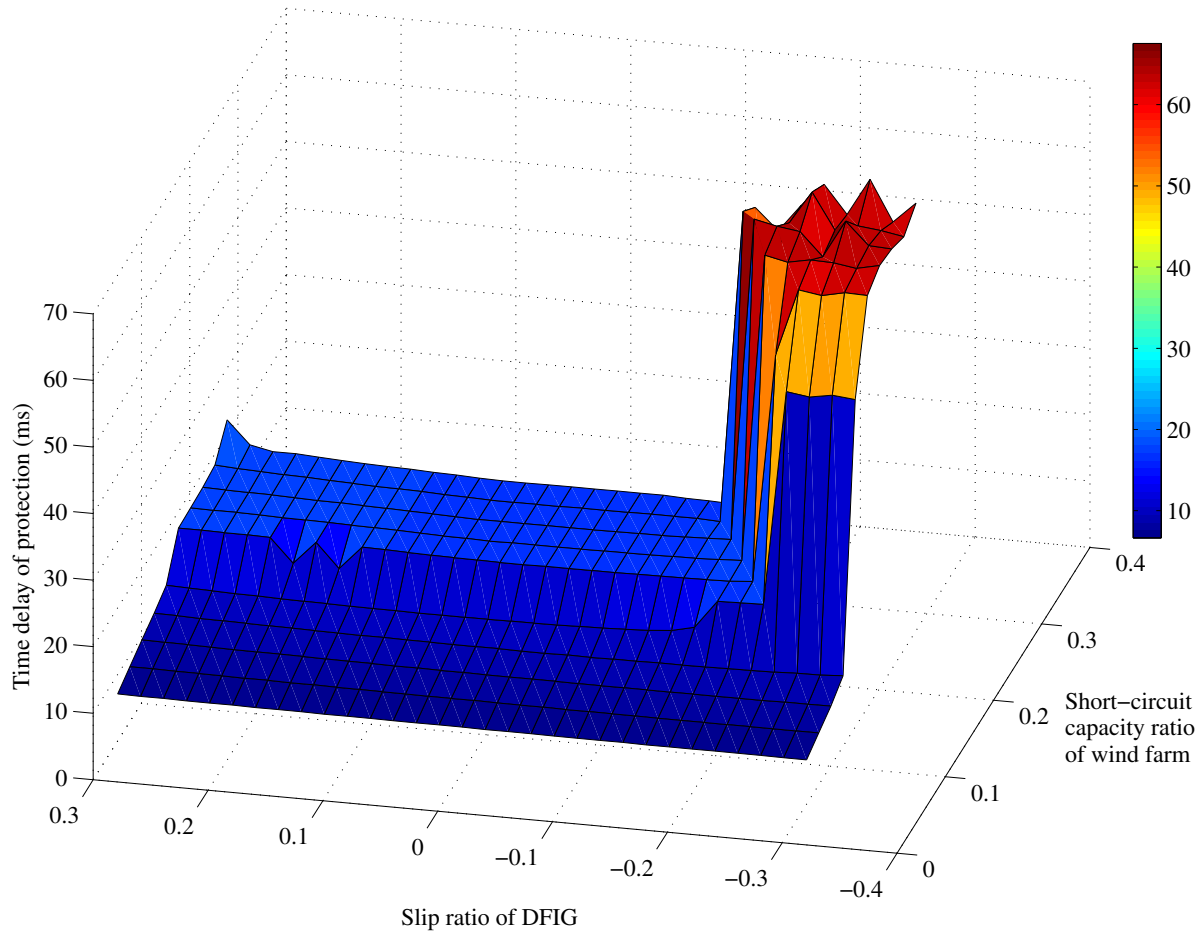


*4.2. Suggestions*

According to the analysis of the factors affecting the reliability of relay protection, several suggestions on improving the reliability of the protections in wind farms are provided as follows.

(1) Increasing the setting value of the second harmonic restraint protection: Increasing the setting values of $K$ from 0.12 to 0.15, the similar relationship between the time delay of the protection with the DFIG's slip ratio and the short-circuit capacity ratio can be plotted as shown in Figure 13. Comparing the results given in Figures 12 and 13, it is clear that the time delay is shortened when the setting value of $K$ is increased. Therefore, the reliability of the protection can be improved by increasing the setting value of the second harmonic restraint protection suitably.

(2) Decreasing the setting value of the over-current differential protection: With the same simulation system for Figure 9, different setting values of the over-current differential protection are selected, and the simulation results are shown in Figure 14, in which $I_e$ is the rated current of the outgoing transformer. As can be seen from the figure, the over-current differential protection would not be activated when the setting value equals $7I_e$. As the setting value decreased to $5I_e$, the over-current differential protection would be activated with a 15-ms delay after the fault occurs.

**Figure 13.** Time delay of the protection with the setting value of $K$ selected as 0.15.

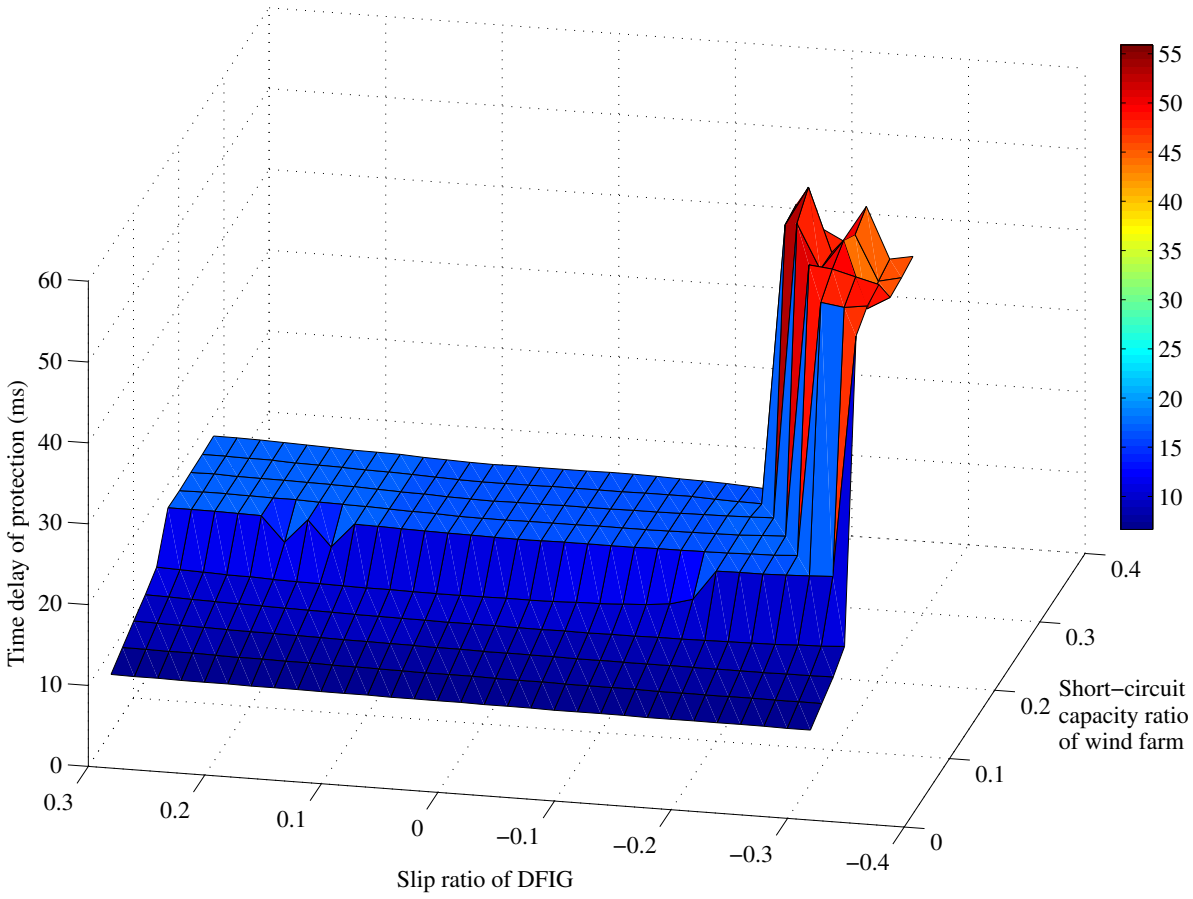


**Figure 14.** Differential current and different setting values of the over-current protection.

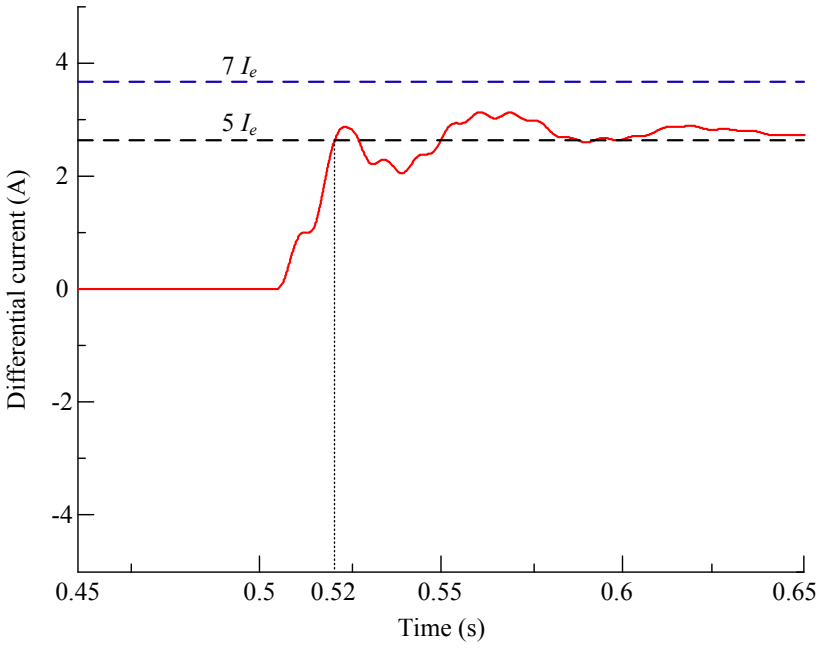

(3) Constraining the slip ratio of the DFIG wind turbines within an acceptable range:

According to the analysis in the last subsection, DFIG-based wind turbines operated in a super-synchronous mode could deteriorate the reliability of the relay protection, while a sub-synchronous one brings much less pressure to relay protection. Therefore, constraining the slip ratio of the DFIGs in a suitable range can improve the reliability of the differential protection for wind farms.

## 5. Conclusions

Crowbar-protected DFIG wind turbines can provide a short-circuit current in the frequency related to their operating conditions in the case of an outgoing transmission line fault occurring. This paper analyzes the frequency characteristics during faults and verifies that, because of the frequency inconsistency, constraint current and differential current fluctuate wildly, which could lead to the incorrect operation of the differential protection. To improve the reliability of the differential protection, several suggestions on how to improve the reliability of the protections in large wind farms are presented. The analysis results and suggestions provided in this paper can be referred to for a relay protection design for DFIG-based wind farms. Additionally, the analysis technique regarding the frequency inconsistency during faults can be employed for other protections for wind farms, such as distance protection.

To simplify the study, we assume that all of the wind generators in the wind farm are identical. However, typically wind generators in a large-scale wind farm are highly diversified, and the individual wind farm protection schemes will activate at different time frames. In our future work, attention will be paid to this aspect.

## Acknowledgments

The authors would like to thank the financial support from the National Science Foundation of China (NSFC) with No. 11102039, the High Technology Research and Development Program (863 Program) of China (2012AA050203) and the Natural Science Foundation of Jiangsu Province with No. BK20140872.

## Author Contributions

Bingtuan Gao, Ning Chen and Yi Tang contributed in developing the ideas of this research. Bingtuan Gao, Wei Wei, Luoma Zhang and Yingjun Wu performed this research. All of the authors were involved in preparing this manuscript.

## Conflicts of Interest

The authors declare no conflict of interest.

## References

1. Marden, J.R.; Ruben, S.D.; Pao, L.Y. A model-free approach to wind farm control using game theoretic methods. *IEEE Trans. Control Syst. Technol.* **2013**, *21*, 1207–1214.

2. Tang, Y.; He, H.; Ni, Z.; Wen, J.; Sui, X. Reactive power control of grid-connected wind farm based on adaptive dynamic programming. *Neurocomputing* **2014**, *125*, 125–133.
3. Zhang, B.; Wang, J.; Li, G.; Hao, Z.; Liu, Z.; Bo, Z. Cooperation of relay protection for grid-connected wind power with low-voltage ride-through capability. *Electr. Power Autom. Equip.* **2012**, *32*, 1–6.
4. Zhang, B.; Zhang, J.; Yuan, B.; Wang, J.; Hao, Z. Impact of wind farm integration on relay protection (6): Analysis of distance protection for wind farm outgoing transmission line. *Electr. Power Autom. Equip.* **2013**, *33*, 1–6.
5. Pannell, G.; Atkinson, D.J.; Zahawi, B. Minimum-threshold crowbar for a fault-ride-through grid-code-compliant DFIG wind turbine. *IEEE Trans. Energy Convers.* **2010**, *25*, 750–759.
6. Erlich, I.; Wrede, H.; Feltes, C. Dynamic Behavior of DFIG-Based Wind Turbines During Grid Faults. In Proceedings of the Power Conversion Conference, Nagoya, Japan, 2–5 April 2007; pp. 1195–1200.
7. Ekanayake, J.B.; Holdsworth, L.; Wu, X.; Jenkins, N. Dynamic modelling of doubly fed induction generator wind turbines. *IEEE Trans. Power Syst.* **2003**, *18*, 803–809.
8. Morren, J.; de Haan, S.W.H. Short-circuit current of wind turbines with doubly fed induction generator. *IEEE Trans. Energy Convers.* **2007**, *22*, 174–180.
9. Li, G.; Zhang, B.; Wang, J.; Bo, Z.; Yip, T.; Writer, D.; Lei, Y. DFIG-Based Wind Farm Electromagnetic Dynamic Model and Impact on Protection Relay of Transmission Network. In Proceedings of the International Conference on Advanced Power System Automation and Protection, Beijing, China, 16–20 October 2011; pp. 694–698.
10. Sideratos, G.; Hatziargyriou, N.D. An advanced statistical method for wind power forecasting. *IEEE Trans. Power Syst.* **2007**, *22*, 258–265.
11. Ma, L.; Luan, S.; Jiang, C.; Liu, H.; Zhang, Y. A review on the forecasting of wind speed and generated power. *Renew. Sustain. Energy Rev.* **2009**, *13*, 915–920.
12. Hansena, A.D.; Sorensena, P.; Iovb, F.; Blaabjerg, F. Centralised power control of wind farm with doubly fed induction generators. *Renew. Energy* **2006**, *31*, 935–951.
13. Gouvalas, N.K.; Gonos, I.F.; Stathopulos, I.A. Impact study of short-circuit calculation methods on the design of a wind farm's grounding system. *Renew. Energy* **2014**, *66*, 25–32.
14. Cho, S.; Shin, H.; Kim, J. Study on coordination of protective relays between primary feeder and interconnecting transformer grounded by SFCL of wind Farm. *IEEE Trans. Appl. Superconduct.* **2012**, *22*, 5500404:1–5500404:4.
15. Xiang, D.; Ran, L.; Tavner, P.J.; Yang, S. Control of a doubly fed induction generator in a wind turbine during grid fault ride-through. *IEEE Trans. Energy Convers.* **2006**, *21*, 652–662.
16. Causebrook, A.; Atkinson, D.J.; Jack, A.G. Fault ride-through of large wind farms using series dynamic braking resistors (March 2007). *IEEE Trans. Power Syst.* **2007**, *22*, 966–975.
17. Okedu, K.E.; Muyeen, S.M.; Takahashi, R.; Tamura, J. Wind farms fault ride through using DFIG with new protection scheme. *IEEE Trans. Sustain. Energy* **2012**, *3*, 242–254.
18. Qureshi, W.A.; Nair, N.C. Wind Farm Protection. In *Large Scale Renewable Power Generation: Advances in Technologies for Generation, Transmission and Strorage*; Hossian, J., Mahmud, A., Eds.; Springer: Singapore, 2014; pp. 311–330.

19. Sarajcev, P.; Goic, R. A review of current issues in state-of-art of wind farm overvoltage protection. *Energies* **2011**, *4*, 644–668.
20. Sadeghi, H. A novel method for adaptive distance protection of transmission line connected to wind farms. *Electr. Power Energy Syst.* **2012**, *43*, 1376–1382.
21. Guajardo, L.A.T.; Enriquez, A.C. Wind Power Plants and FACTS Devices' Influence on the Performance of distance Relays. In *Large Scale Renewable Power Generation: Advances in Technologies for Generation, Transmission and Strorage*; Hossian, J., Mahmud, A., Eds.; Springer: Singapore, 2014; pp. 331–368.
22. Horowitz, S.H.; Phadke, A.G. *Power System Relaying*; Research Studies Press Limited and John Wiley & Sons Ltd.: West Sussex, UK, 1994; pp. 195–223.
23. Guzman, A.; Altuve, H.J.; Benmouyal, G. Power Transformer Protection. In *Electric Power Transformer Engineering*; Harlow, J.H., Ed.; CRC Press Taylor & Francis Group: Boca Raton, FL, USA, 2004; pp. 353–381.
24. Zhang, W.; Tan, Q.; Miao, S.; Zhou, L.; Liu, P. Self-adaptive transformer differential protection. *IET Gener. Transm. Distrib.* **2013**, *7*, 61–68.
25. Oliveira, M.O.; Breta, A.S.; Ferreira, G.D. Adaptive differential protection of three-phase power transformers based on transient signal analysis. *Electr. Power Energy Syst.* **2014**, *57*, 366–374.
26. Zhang, B.; Wang, J.; Hao, Z.; Mo, L.; Yan, K.; Wang, X. Impact of wind farm integration on relay protection (3): Performance analysis for wind farm outgoing transformer protection. *Electr. Power Autom. Equip.* **2013**, *33*, 1–8.
27. Wei, W.; Zhang, L.; Gao, B.; Tang, Y.; Chen, N.; Zhu, L. Frequency Inconsistency in DFIG-Based Wind Farm during Outgoing Transmission Line Faults and Its Effect on Longitudinal Differential Protection. In Proceedings of IEEE International Conference on CYBER Technology in Automation, Control, and Intelligent Systems, Hong Kong, China, 4–7 June 2014; pp. 25–30.
28. Che, Q.; Lu, Y. Research on wind farm relay protection value setting based on crowbar circuit LVRT technology. *Power Syst. Prot. Control* **2013**, *41*, 97–102.